Calculation and Experimental Measurement of Paramagnetic NMR Parameters of Phenolic Oximate Cu(II) Complexes

Daniel M. Dawson, Zhipeng Ke, Frederick M. Mack, Rachel A. Doyle,
Giulia P. M. Bignami, Iain A. Smellie, Michael Bühl and Sharon E. Ashbrook

School of Chemistry, EaStCHEM and Centre for Magnetic Resonance, University of St Andrews, North Haugh, St Andrews KY16 9ST, UK

Supporting Information

S1. Synthesis and Basic Characterisation of Oximes and Cu(II) Complexes

S2. Computational Details

S3. Solid-State NMR Details

S4. One- and Two-Dimensional Solid-State NMR Spectra of 2-5 and 7-9.

S5. Final Assignments of ^{1}H and ^{13}C NMR Spectra of 2-5 and 7-9.

S6. Vibrational Effects on the pNMR Parameters of 1

S7. References

S1. Synthesis and Basic Characterisation of Oximes and Cu(II) Complexes

Synthesis of the oximes

All oxime ligands (denoted H**LN**, using the numbering scheme of the main text) were prepared using the same general protocol. The commercially-available starting aldehyde or ketone (15 mmol) was dissolved in 80% aqueous ethanol (40 cm^3). This was mixed with sodium acetate (37 mmol) and hydroxylamine hydrochloride (30 mmol) was dissolved in water (10 cm^3) and then heated under reflux for 3 h. The solvent was removed *in vacuo* and water (20 cm^3) was added to the crude residue. The product was extracted using ethyl acetate (3 × 20 cm^3) and the three organic fractions were combined and washed with brine (3 × 15 cm^3). The organic layers were dried over anhydrous sodium sulfate and the solvent was removed *in vacuo*. The crude product was recrystallized from boiling 60-80 petroleum ether (20 cm^3), with the addition of small portions of ethyl acetate if required.

As previously reported,[S1] H**L1** was obtained in 52% yield (mp. 56.2–58.3 °C lit. 56.1-58.1 °C[S2]). ^{1}H NMR: δH (400.13 MHz, $CDCl_3$, Me_4Si): 9.79 (1H, s, C-OH), 8.24 (1H, t, J = 0.4 Hz, H7), 7.30 (1H, s, N-OH), 7.29 (1H, ddd, J = 8.3, 7.3, 1.7 Hz, H5), 7.19 (1H, ddt, J = 7.7, 1.7, 0.4 Hz, H3), 6.99 (1H, ddt, J = 8.3, 1.2, 0.4 Hz, H6), 6.93 (1H, ddd, J = 7.5, 7.4, 1.2 Hz, H4). ^{13}C{^{1}H} NMR: δC (100.66 MHz, $CDCl_3$, Me_4Si): 157.3 (C1), 153.2 (C7), 131.5 (C5), 130.9 (C3), 119.9 (C4), 116.9 (C6) and 116.4 (C2).

H**L2** was obtained in 37% yield (mp. 117.7-120.0 °C lit. 112 °C[S3]). ^{1}H NMR: δH (400.13 MHz, $CDCl_3$, Me_4Si) 11.49 (1H, s, C-OH), 7.81 (1H, br s, N-OH), 7.45 (1H, ddd, J = 8.0, 1.6, 0.3 Hz, H6), 7.28 (1H, ddd, J = 8.2, 7.3, 1.6 Hz, H4), 6.99 (1H, ddd, J = 8.2, 1.3, 0.3 Hz, H3), 6.92 (1H, ddd, J = 8.0, 7.3, 1.3 Hz, H5), 2.37 (3H, s, H8). ^{13}C{^{1}H} NMR: δC (75.5 MHz, $CDCl_3$, Me_4Si) 159.6 (C7), 157.5 (C1), 130.9 (C6), 127.8 (C4), 119.5 (C3), 118.7 (C1), 117.4 (C5), 10.9 (C8).

H**L3** was obtained in 43% yield (mp. 156.1-160.1 °C lit. 148.0-150.0 °C[S4]). ^{1}H NMR: δH (400.13 MHz, $CDCl_3$, Me_4Si) 10.86 (1H, s, C-OH), 9.15 (1H, t, J = 0.5 Hz, H7), 7.97 (1H, dm, J

= 8.5 Hz, ArH), 7.80 (1H, dm, J = 9.0 Hz, ArH), 7.79 (1H, dm, J = 8.1 Hz), 7.53 (1H, ddd, J = 8.5, 6.9, 1.4 Hz, ArH), 7.38 (1H, ddd, J = 8.0, 6.9, 1.1 Hz, ArH), 7.32 (1H, br s, N-OH), 7.22 (1H, dm, J = 9.0 Hz, ArH). $^{13}C\{^{1}H\}$ NMR: δC (75.5 MHz, $CDCl_3$, Me_4Si) 157.4 (C2), 149.9 (C7), 132.6 (CH), 131.9 (C5/6), 129.0 (CH), 128.3 (C5/6), 127.5 (CH), 123.6 (CH), 120.2 (CH), 118.8 (CH), 106.8 (C1).

H**L4** was obtained in 56% yield (mp. 120.0-121.4 °C lit. 121 °C[S5]). ^{1}H NMR: δH (400.13 MHz, $CDCl_3$, Me_4Si) 10.0 (1H, s(br), C-OH), 8.23 (1H, s, N-OH), 6.93-6.81 (3H, m, H4+5+6), 3.90 (3H, s, H8). $^{13}C\{^{1}H\}$ NMR: δC (75.5 MHz, $CDCl_3$, Me_4Si) 152.6 (C7), 148.2 (C2), 146.9 (C3), 122.4 (C4/6), 119.6 (C4/6), 116.8 (C1), 113.3 (C5), 56.1 (C8).

As previously reported,[S6] H**L5** was obtained in 37% yield (mp. 116-117 °C lit. 116.0-116.5 °C[S7]). ^{1}H NMR: δH (400.13 MHz, $CDCl_3$, Me_4Si) 9.68 (1H, s, C-OH), 8.24 (1H, dd, J = 0.5, 0.4 Hz, H7), 7.40 (1H, s, N-OH), 7.33 (1H, dd, J = 8.6, 2.5 Hz, H4), 7.15 (1H, ddd, J= 2.5, 0.4, 0.4 Hz H6), 6.93 (1H, ddd, J= 8.6, 0.5, 0.4 Hz H3), 1.30 (9H, s, H9). $^{13}C\{^{1}H\}$ NMR: δC (75.5 MHz, $CDCl_3$, Me_4Si) 155.1 (C2), 153.7 (C7), 142.6 (C5), 128.8 (C4/6), 127.5 (C4/6), 116.4 (C3), 115.7 (C1), 34.1 (C8), 31.5 (C9).

H**L6** was obtained in 77% yield (mp. 117.8-119.6 °C lit. 122 °C[S8]). ^{1}H NMR: δH (400.13 MHz, $CDCl_3$, Me_4Si) 9.41 (1H, s, C-OH), 8.18 (1H, dd, J = 0.4, 0.4 Hz, H7), 7.43 (1H, s, NOH), 6.92 (1H, m, H3/4), 6.88 (1H, m, H3/4), 6.69 (1H, dt, J = 2.8, 0.4 Hz, H6), 3.78 (3H, s, H8).

H**L7** was obtained in 83% yield (mp. 138.0-139.6 °C lit. 136 °C[S9]). ^{1}H NMR: δH (400.13 MHz, $CDCl_3$, Me_4Si) 10.0 (1H, s, C-OH), 8.19 (1H, dd, J = 0.4, 0.4 Hz, H7), 7.22 (1H, s, br, NOH), 7.10 (1H, m, H6), 6.54 (1H, m, H3), 6.51 (1H, m, H5), 3.83 (3H, s, OCH_3).

H**L8** was obtained in 43% yield (mp. 127.0-130.0 °C lit. 133-134.5 °C[S10]). ^{1}H NMR: δH (400.13 MHz, $CDCl_3$, Me_4Si) 9.79 (1H, s, C-OH), 8.15 (1H, dd, J = 0.4, 0.4 Hz, H7), 7.37 (1H, s, br, N-OH), 7.37 (1H, dd, J = 8.8, 2.5 Hz, H4), 7.30 (1H, ddd, J = 2.4, 0.4, 0.4 Hz, H6), 6.88

(1H, ddd, J= 8.8, 0.4, 0.4 Hz, H3). $^{13}C\{^{1}H\}$ NMR: δC (125.8 MHz, $CDCl_3$, Me_4Si) 156.5 (C2), 152.0 (C7), 134.1 (C4), 133.0 (C6), 118.8 (C3), 118.1 (C1), 111.4 (C5).

H**L9** was obtained in 85% yield (mp. 115.0-116.2 °C lit. 100 °C[S8]). ^{1}H NMR: δH (400.13 MHz, $CDCl_3$, Me_4Si) 9.86 (1H, s, C-OH), 8.24 (1H, s, H7), 7.86 (1H, s, br, NOH), 6.93-6.92 (3H, m, H4+5+6), 4.13 (2H, q, J = 7.0 Hz, H8), 1.48 (3H, t, J= 7 Hz, H9).

Synthesis of the bis(oximato)copper(II) complexes

Bis(oximato)copper(II) complexes (with formula Cu(**LN**)$_2$, denoted **N**, using the numbering scheme of the main text) were prepared using the following general protocol. The prepared ligand (1 mmol) in ethanol (12 cm^3) was added to a hot solution of 0.02 M aqueous copper sulfate (25 cm^3, 0.5 mmol). The mixture was stirred for 15 minutes to afford a pale green-brown precipitate, which was washed with water and dried in air. Powder X-ray diffraction data were collected on a STOE STADIP instrument operated in capillary Debye-Scherrer mode equipped with a Cu X-ray tube, a primary beam monochromator ($CuK_{\alpha1}$) and a scintillation position-sensitive linear detector. 2θ ranges of 3-70° were investigated over 16 h of acquisition time and samples were packed in 0.7 mm glass capillaries.

1 was obtained in 47% yield. Fig. S1.1 shows the pXRD pattern of **1** and the simulated pXRD patterns for the two known polymorphs,[S11] with CSD entry codes SALCOP03 (polymeric [Cu(**L1**)$_2$]$_n$) and SALCOP04 (monomeric Cu(**L1**)$_2$), confirming the monomeric nature of this sample.

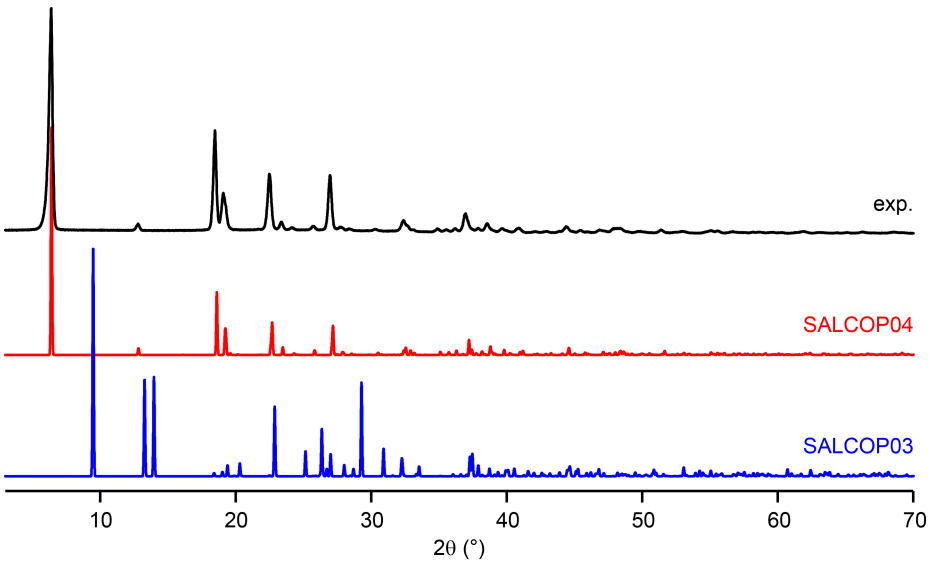

Fig. S1.1. Experimental pXRD pattern of **1** and patterns simulated for CSD entries SALCOP03 and SALCOP04[S11].

2 was obtained in 49% yield. Fig. S1.2 shows the pXRD pattern of **2**.

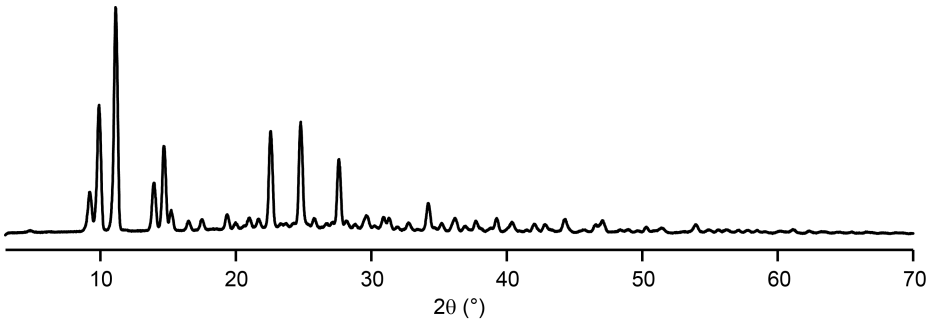

Fig. S1.2. Experimental pXRD pattern of **2**.

3 was obtained in 91% yield. Fig. S1.3 shows the pXRD pattern of **3**.

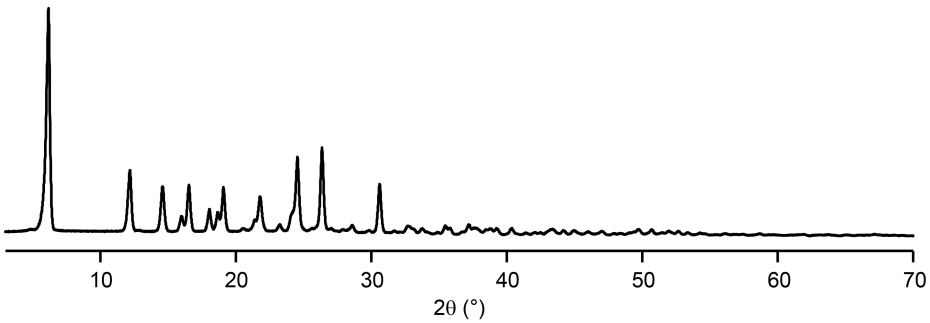

Fig. S1.3. Experimental pXRD pattern of **3**.

4 was obtained in 86% yield. Fig. S1.4 shows the pXRD pattern of **4**.

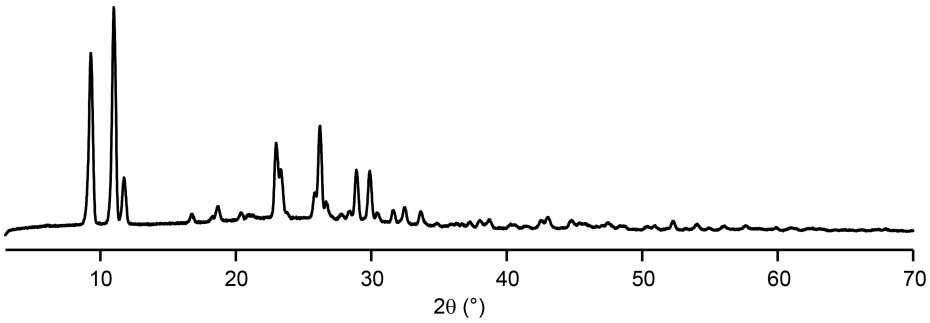

Fig. S1.4. Experimental pXRD pattern of **4**.

5 was obtained in 27% yield. Fig. S1.5 shows the pXRD pattern of **5**.

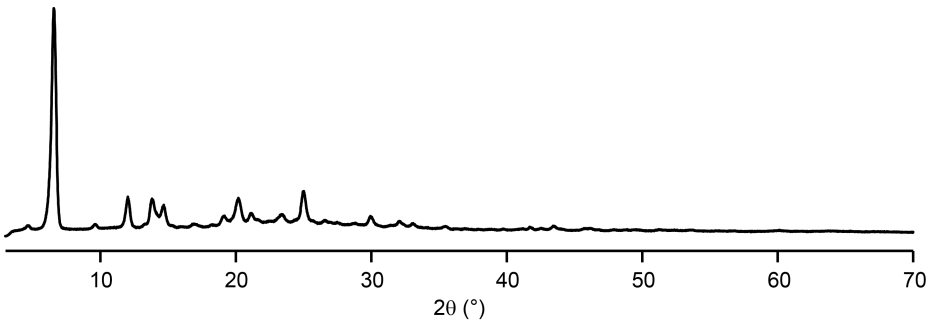

Fig. S1.5. Experimental pXRD pattern of **5**.

6 was obtained in 68% yield. Fig. S1.6 shows the pXRD pattern of **6**.

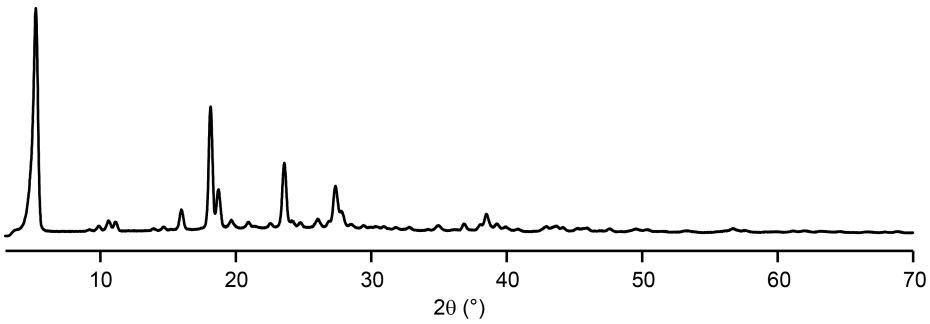

Fig. S1.6. Experimental pXRD pattern of **6**.

7 was obtained in 76% yield. To obtain the polymorph of **7** discussed in the text, the sample was heated at 110 °C overnight.[S12] Fig. S1.7 shows the pXRD patterns of **7** before and after heating.

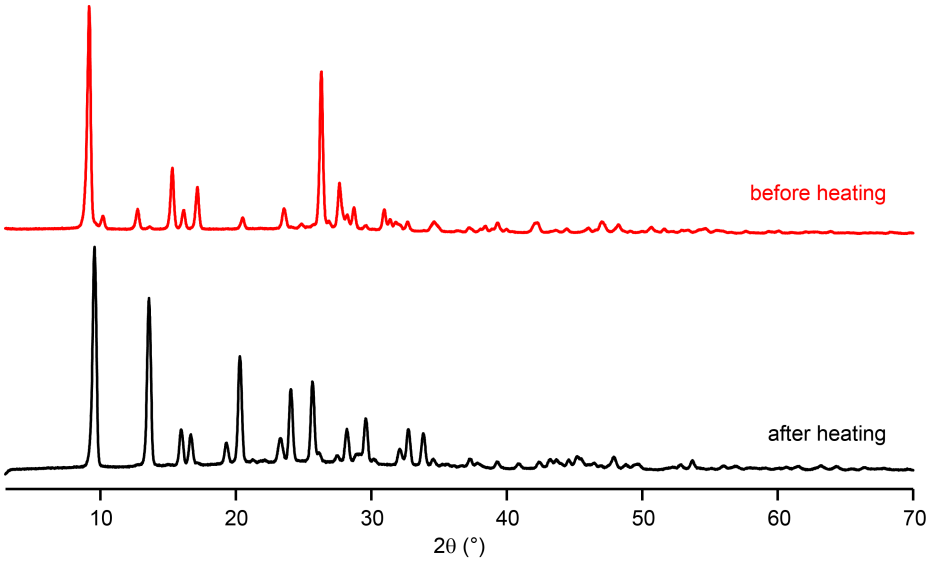

Fig. S1.7. Experimental pXRD patterns of **7** before (red) and after (black) heating at 110 °C overnight.

8 was obtained in 75% yield. Fig. S1.8 shows the pXRD pattern of **8**.

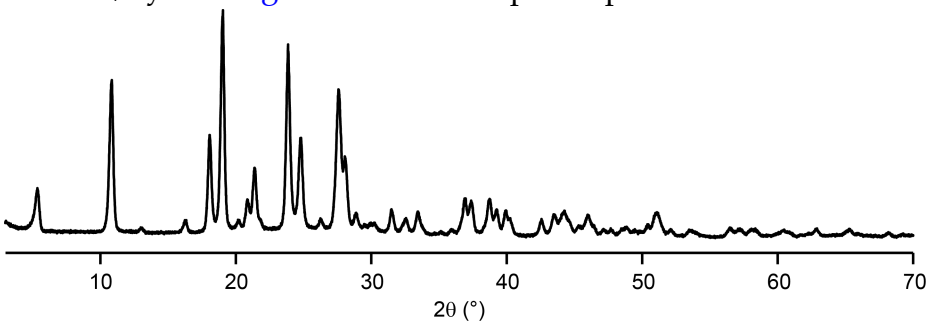

Fig. S1.8. Experimental pXRD pattern of **8**.

9 was obtained in 70% yield. Fig. S1.9 shows the pXRD pattern of **9**.

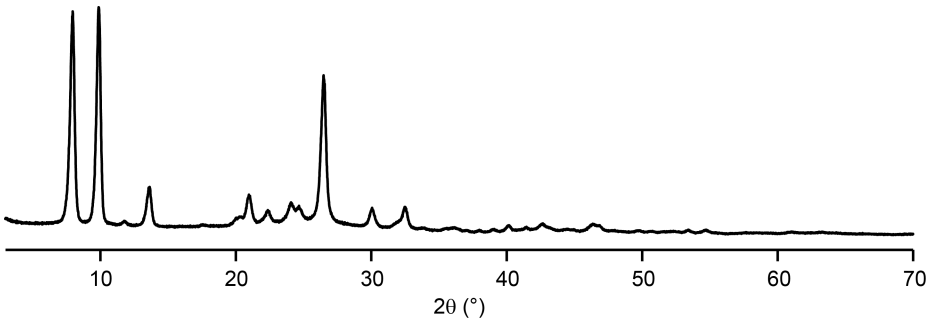

Fig. S1.9. Experimental pXRD pattern of **9**.

S2. Computational Details

The calculation of pNMR parameters employed the methodology introduced in Ref. S1; *i.e.*, structures were optimised with the Gaussian 09[S13] at the PBE0-D3[S14-S20] level of density functional theory, employing a Wachters basis[S21,S22] augmented with two diffuse *p* and one diffuse *d* sets for Cu (8s7p4d), 6-31G** for the H(br) atoms and 6-31G* for all other atoms. The σ_{orb}, g and A tensors were computed at the PBE0-1/3[S23] level using a 9s7p4d basis set on Cu that was constructed specifically for hyperfine coupling constant calculations,[S24] and the IGLO-II basis[S25] on the ligands. The σ_{orb} calculations employed gauge-including atomic orbitals and fine integration grids as implemented in Gaussian 09. The g and A tensors were computed with ORCA[S26] (tight SCF convergence and fine integration grid, Grid5 option). Isotropic magnetic shielding constants σ_{iso} were computed using the formalism given in Ref. S27, where the effective spin (1/2 in our case), the temperature (set to 298.15 K), and the isotropic and anisotropic parts of the A and g tensors enter explicitly. Chemical shifts δ_{iso} are reported relative to TMS according to $\delta_{iso} = \sigma_{orb}(TMS) - \sigma_{iso}$, where the isotropic orbital shieldings of TMS have been computed at the same level.

As described in the main text, the partial s character of the HOMO on atoms close to the Cu leads to large computed hyperfine couplings for these nuclei. As an example, Table S2.1 gives the contributions from C and H to the α-HOMO for **6**.

Table S2.1. Orbital coefficients for C and H (PBE0-1/3 / IGLO-II) for the α-HOMO of **6**.[a]

Atom	Orbital	Occupancy	Atom	Orbital	Occupancy	Atom	Orbital	Occupancy
H3	1S	0.00417	C2	1S	–0.00232	C6	1S	0.00338
	2S	0.00712		2S	–0.00353		2S	0.00495
	3S	0.00371		3S	–0.00040		3S	0.00138
	4PX	0.00102		4S	0.00812		4S	–0.01508
	4PY	–0.00046		5S	0.04326		5S	–0.03702
	4PZ	0.00000		6PX	–0.01129		6PX	–0.00175
H4	1S	–0.01430		6PY	–0.00481		6PY	0.00262
	2S	–0.02492		6PZ	0.00000		6PZ	0.00000
	3S	–0.01319		7PX	–0.03754		7PX	–0.00481
	4PX	0.00115		7PY	–0.01358		7PY	0.00781
	4PY	–0.00053		7PZ	0.00000		7PZ	0.00000
	4PZ	0.00000		8PX	–0.03334		8PX	–0.00901
H6	1S	0.00866		8PY	–0.02481		8PY	0.00979
	2S	0.01770		8PZ	0.00000		8PZ	0.00000
	3S	0.01633		9PX	–0.05697		9PX	0.01088
	4PX	–0.00007		9PY	0.03514		9PY	0.03933
	4PY	–0.00037		9PZ	0.00000		9PZ	0.00000
	4PZ	0.00000	C3	1S	0.01001	C7	1S	0.01020
H7	1S	0.03191		2S	0.01415		2S	0.01480
	2S	0.06192		3S	0.00550		3S	0.00470
	3S	0.05814		4S	–0.04972		4S	–0.05270
	4PX	0.00274		5S	–0.10215		5S	–0.06639
	4PY	–0.00005		6PX	0.01120		6PX	–0.00529
	4PZ	0.00000		6PY	0.01078		6PY	0.01038
H8	1S	–0.00093		6PZ	0.00000		6PZ	0.00000
	2S	–0.00125		7PX	0.03261		7PX	–0.01636
	3S	–0.00166		7PY	0.03254		7PY	0.03041
	4PX	0.00012		7PZ	0.00000		7PZ	0.00000
	4PY	0.00009		8PX	0.05884		8PX	–0.01787
	4PZ	0.00021		8PY	0.04965		8PY	0.04870
H8′	1S	0.00147		8PZ	0.00000		8PZ	0.00000
	2S	0.00313		9PX	0.02417		9PX	–0.03701
	3S	0.00053		9PY	–0.04716		9PY	–0.02737
	4PX	0.00002		9PZ	0.00000		9PZ	0.00000
	4PY	0.00031	C4	1S	–0.00373	C8	1S	0.00038

	4PZ	0.00000		2S	–0.00554	2S	0.00053
H8′′	1S	–0.00093		3S	–0.00138	3S	0.00021
	2S	–0.00125		4S	0.01540	4S	–0.00207
	3S	–0.00166		5S	0.05598	5S	–0.00251
	4PX	0.00012		6PX	–0.00258	6PX	–0.00032
	4PY	0.00009		6PY	–0.00637	6PY	–0.00050
	4PZ	–0.00021		6PZ	0.00000	6PZ	0.00000
Hbr	1S	–0.01873		7PX	–0.0075	7PX	–0.00099
	2S	–0.03642		7PY	–0.01792	7PY	–0.00167
	3S	0.03106		7PZ	0.00000	7PZ	0.00000
	4PX	–0.00065		8PX	–0.01200	8PX	–0.00082
	4PY	–0.01156		8PY	–0.03076	8PY	–0.00165
	4PZ	0.00000		8PZ	0.00000	8PZ	0.00000
C1	1S	–0.00508		9PX	0.00708	9PX	–0.00019
	2S	–0.00724		9PY	–0.05525	9PY	–0.00258
	3S	–0.00266		9PZ	0.00000	9PZ	0.00000
	4S	0.02421	C5	1S	–0.00027		
	5S	0.05209		2S	–0.00036		
	6PX	0.01351		3S	–0.00021		
	6PY	–0.00537		4S	0.00155		
	6PZ	0.00000		5S	0.00477		
	7PX	0.03895		6PX	0.00214		
	7PY	–0.01551		6PY	–0.00001		
	7PZ	0.00000		6PZ	0.00000		
	8PX	0.07366		7PX	0.00722		
	8PY	–0.02837		7PY	0.00039		
	8PZ	0.00000		7PZ	0.00000		
	9PX	–0.03755		8PX	0.00701		
	9PY	0.03159		8PY	–0.00186		
	9PZ	0.00000		8PZ	0.00000		
				9PX	0.03805		
				9PY	0.00210		
				9PZ	0.00000		

a. Only occupancies of s and p orbitals are given (enumerated consecutively in the contracted [3s1p] and [5s4p] parts of the H and C basis sets, respectively). Note that the two equivalent ligands have the same s-orbital coefficients, whereas the p orbitals are equal in magnitude but opposite in sign.

S3. Solid-State NMR Details

Solid-state NMR spectra were recorded using a Bruker Avance III spectrometer, equipped with a 14.1 T wide-bore superconducting magnet (at ^{1}H and ^{13}C Larmor frequencies of 600.13 and 150.94 MHz, respectively). Experiments were carried out using a 1.9 mm MAS probe, with MAS rates between 37.5 and 40 kHz. ^{1}H and ^{13}C peak positions are quoted in ppm relative to $(CH_3)_4Si$, using the N**H**$_3$ and C**H**$_3$ resonances of L-alanine (8.5 and 20.5 ppm, respectively) as secondary references. MAS spectra were recorded using a rotor-synchronised spin-echo pulse sequence with an echo duration of one rotor period. Signal averaging was carried out for 128-1024 (^{1}H) or 16384-122880 transients (^{13}C) with a recycle interval of 100 ms in all cases. Where required, frequency-stepped acquisition was carried out with the transmitter offset incremented by ~100 ($\nu_1 \approx 125$ kHz for ^{1}H and ^{13}C) for each sub-spectrum. Heteronuclear correlation spectra were recorded using cross polarisation (CP) from ^{1}H with a contact pulse (ramped for ^{1}H) of 100 μs, and are the result of averaging between 440 and 2048 transients for each of between 16 and 192 t_1 increments of 26.67 μs, with a repeat interval of 100 ms. Where required, sub spectra were recorded at transmitter offsets on resonance for C3+C7/H7 in addition to sub spectra on resonance for all other species. For example, for the spectra in Fig. 4 of the main text transmitter offsets of –9 kHz and 148 kHz (^{1}H) and 20 kHz and 115 kHz (^{13}C) were used. In all experiments, the sample temperature was controlled using a Bruker BCU-II chiller and Bruker BVT/BVTB-3000 temperature controller and heater booster. The sample temperature (including frictional heating effects arising from sample spinning) was calibrated using the isotropic ^{87}Rb shift of solid RbCl.[S28]

S4. One- and Two-Dimensional Solid-State NMR Spectra of 2-5 and 7-9.

Fig. S4.1 shows the ^{1}H and ^{13}C MAS NMR spectra of **2**. The resonances for C3 and C7 (predicted by the calculations to be at 1146 and 951.7 ppm, respectively) are not observed experimentally. Both ^{1}H and ^{13}C T_1 relaxation constants are much smaller for **2** (on the order of 0.5-2 ms for both nuclei, data not presented) than the other complexes, perhaps suggesting that these resonances cannot be observed owing to a loss of signal intensity during the spin echo. Fig. S4.2 shows the ^{1}H-^{13}C CP HETCOR spectrum of **2**.

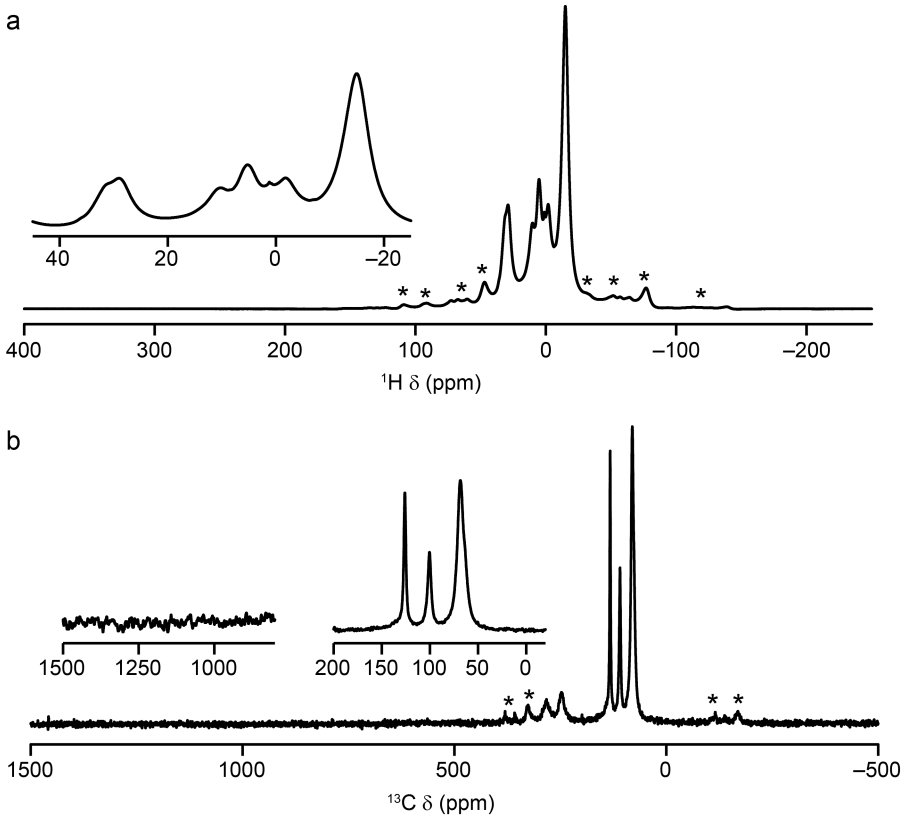

Fig. S4.1. (a) ^{1}H (14.1 T, 298 K, 37.5 kHz MAS) and (b) ^{13}C (14.1 T, 298 K, 37.5 kHz MAS) NMR spectra of **2**. Insets show expansions of closely-spaced resonances and (for ^{13}C) the absence of the expected resonances at high shift. Spinning sidebands are marked by asterisks.

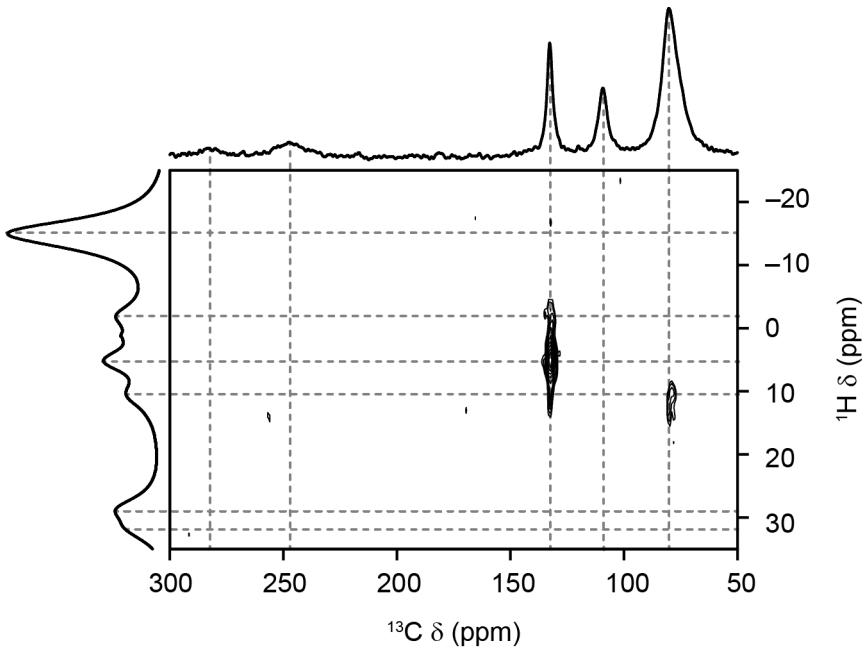

Fig. S4.2. ^{1}H-^{13}C (14.1 T, 298 K, 37.5 kHz MAS) CP HETCOR spectrum of **2**. Owing to the lack of high-frequency resonances in the MAS spectra, only one quadrant of the HETCOR was recorded.

Fig. S4.3 shows the ^{1}H and ^{13}C MAS NMR spectra of **3**. Multiple resonances are observed for some chemically-equivalent sites (*e.g.*, H4 at 35.9 and 33.6 ppm, see Fig. S4.3(a)), indicating crystallographic inequivalence – either the two ligands in the complex are inequivalent, or there are multiple crystallographically-distinct complexes within the unit cell. In the main text, average shifts and temperature dependence parameters were reported where multiple resonances were observed for a given chemical species. The individual shifts are reported in Section S5. Fig. S4.4 shows the ^{1}H-^{13}C CP HETCOR spectrum of **3**.

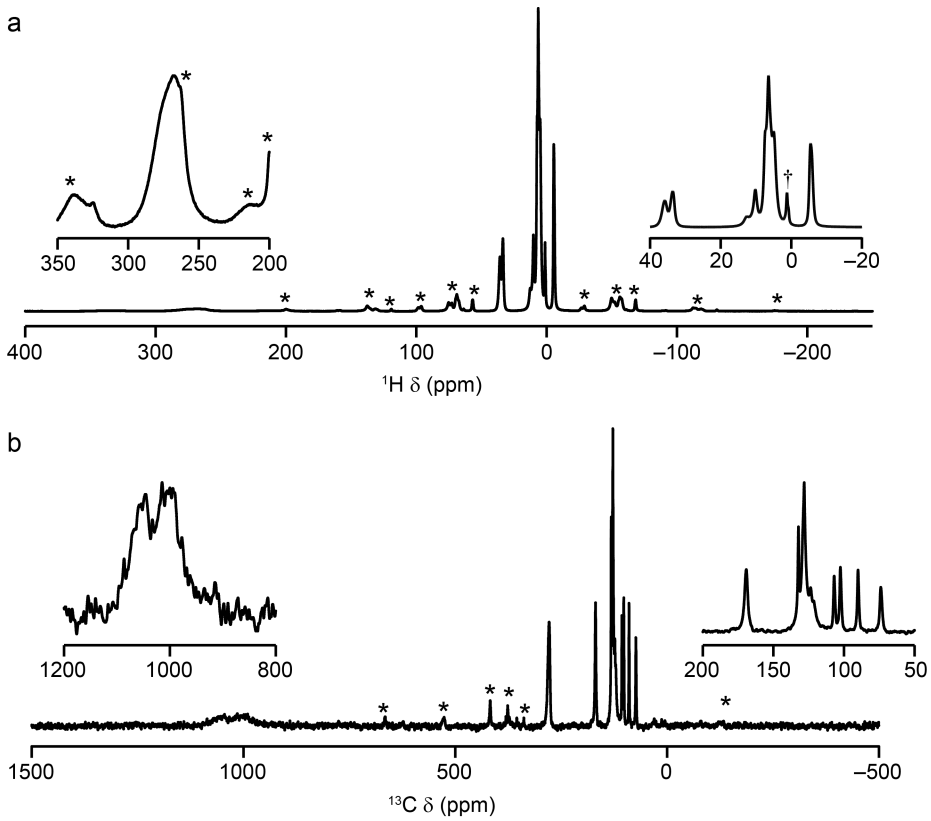

Fig. S4.3. (a) ^{1}H (14.1 T, 298 K, 37.5 kHz MAS) and (b) ^{13}C (14.1 T, 298 K, 37.5 kHz MAS) NMR spectra of **3**. Insets show expansions of the most shifted and more closely-spaced resonances. Spinning sidebands are marked by asterisks and the dagger marks a ^{1}H resonance arising from a contaminant in the rotor cap.

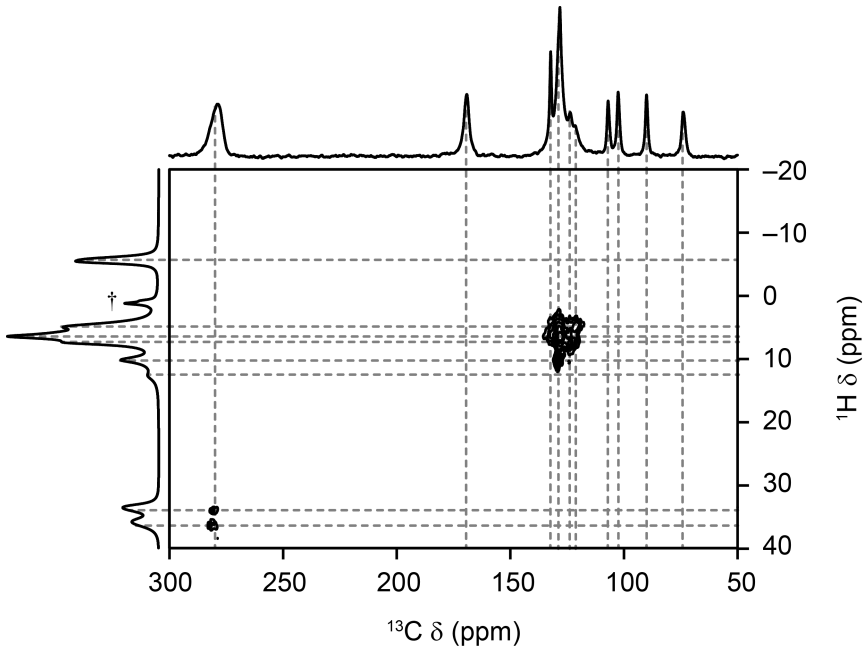

Fig. S4.4. ^{1}H-^{13}C (14.1 T, 298 K, 37.5 kHz MAS) CP HETCOR spectrum of **3**. The dagger marks a ^{1}H resonance arising from a contaminant in the rotor cap.

Fig. S4.5 shows the ^{1}H and ^{13}C MAS NMR spectra of **4**. Fig. S4.6 shows the ^{1}H-^{13}C CP HETCOR spectrum of **4**.

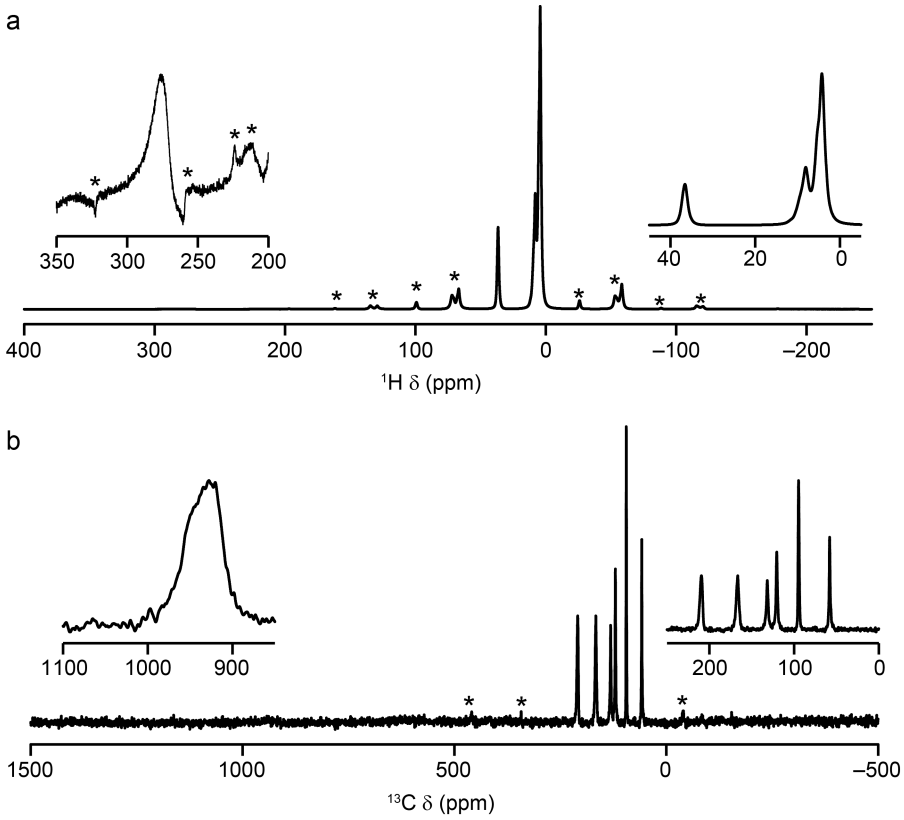

Fig. S4.5. (a) ^{1}H (14.1 T, 298 K, 37.5 kHz MAS) and (b) ^{13}C (14.1 T, 298 K, 37.5 kHz MAS) NMR spectra of **4**. Insets show expansions of the most shifted and more closely-spaced resonances. Spinning sidebands are marked by asterisks.

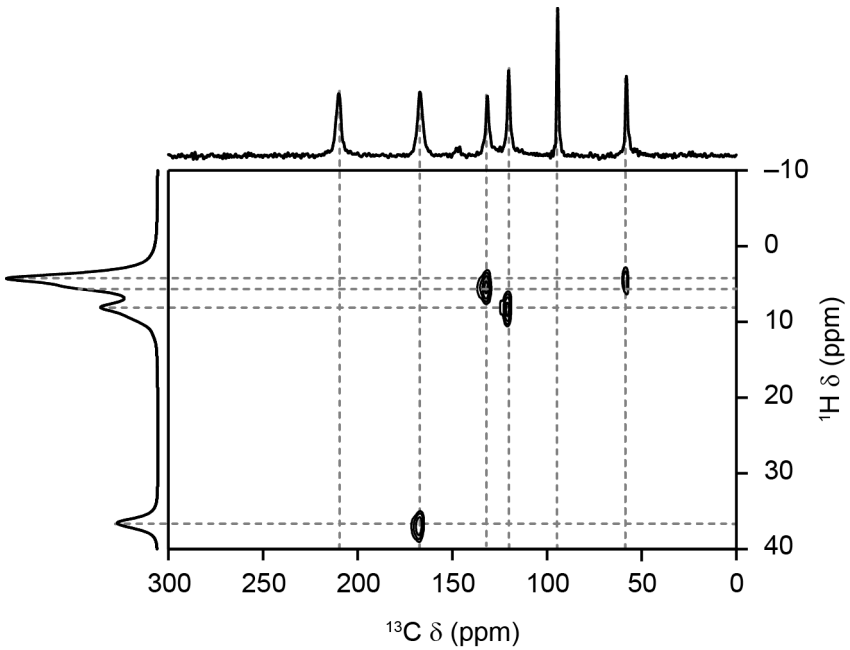

Fig. S4.6. ^{1}H-^{13}C (14.1 T, 298 K, 37.5 kHz MAS) CP HETCOR spectrum of **4**.

Fig. S4.7 shows the ^{1}H and ^{13}C MAS NMR spectra of **5**. The signal for C3 (see inset in Fig. S4.7(b)) is very broad and determining an accurate shift and temperature dependence is challenging. The large experimental errors (see Section S5) lead to the disagreement between experiment and computation in Fig. 5 of the main text. Fig. S4.8 shows the ^{1}H-^{13}C CP HETCOR spectrum of **5**.

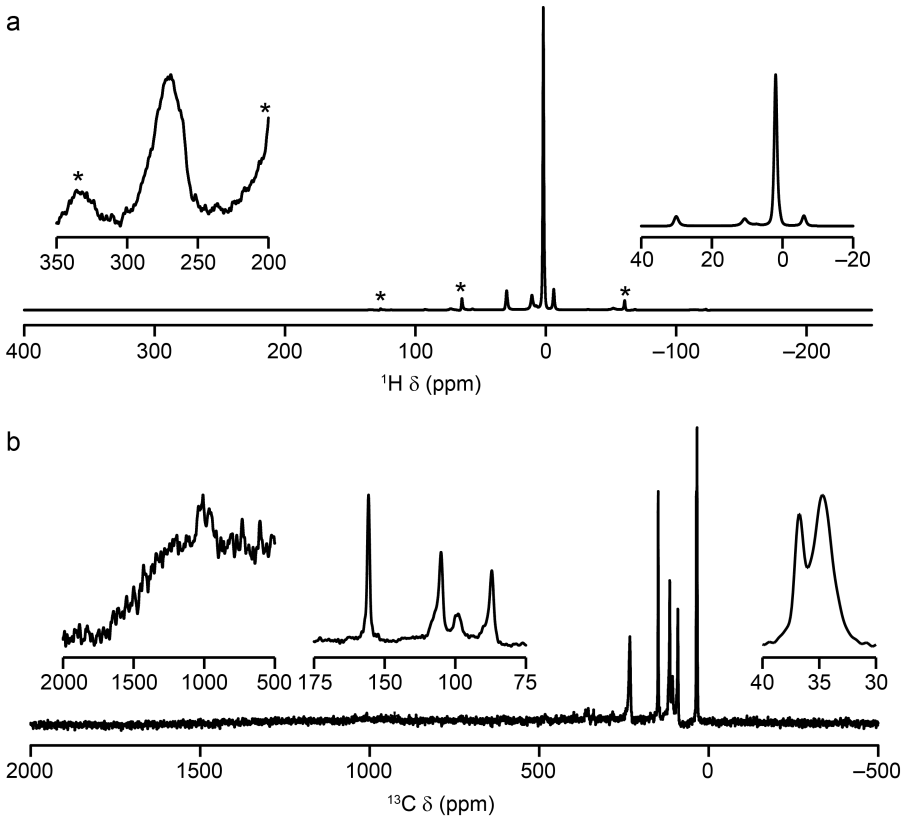

Fig. S4.7. (a) ^{1}H (14.1 T, 298 K, 37.5 kHz MAS) and (b) ^{13}C (14.1 T, 298 K, 37.5 kHz MAS) NMR spectra of **5**. Insets show expansions of the most shifted and more closely-spaced resonances. Spinning sidebands are marked by asterisks.

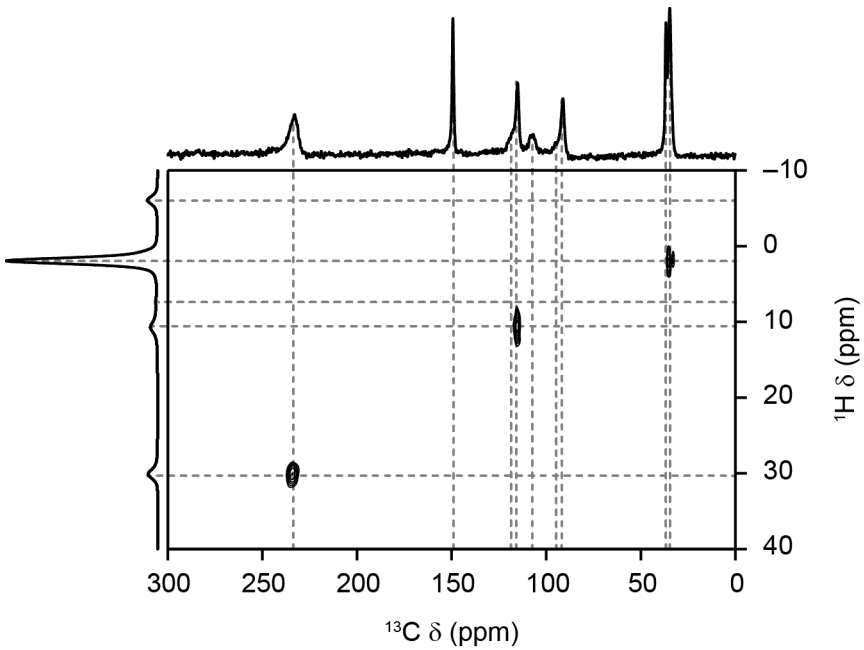

Fig. S4.8. ^{1}H-^{13}C (14.1 T, 298 K, 37.5 kHz MAS) CP HETCOR spectrum of **5**.

Fig. S4.9 shows the ^{1}H and ^{13}C MAS NMR spectra of **7** (after heating at 110 °C overnight). Fig. S4.10 shows the ^{1}H-^{13}C CP HETCOR spectrum of the same sample of **7**.

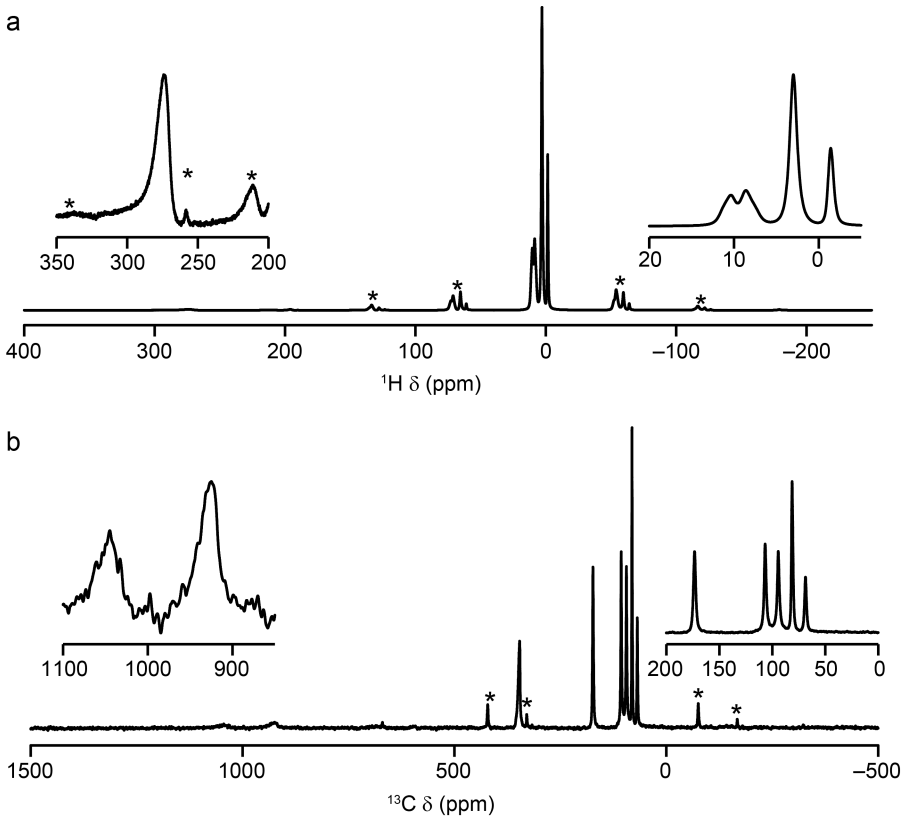

Fig. S4.9. (a) ^{1}H (14.1 T, 298 K, 37.5 kHz MAS) and (b) ^{13}C (14.1 T, 298 K, 37.5 kHz MAS) NMR spectra of **7**. Insets show expansions of the most shifted and more closely-spaced resonances. Spinning sidebands are marked by asterisks.

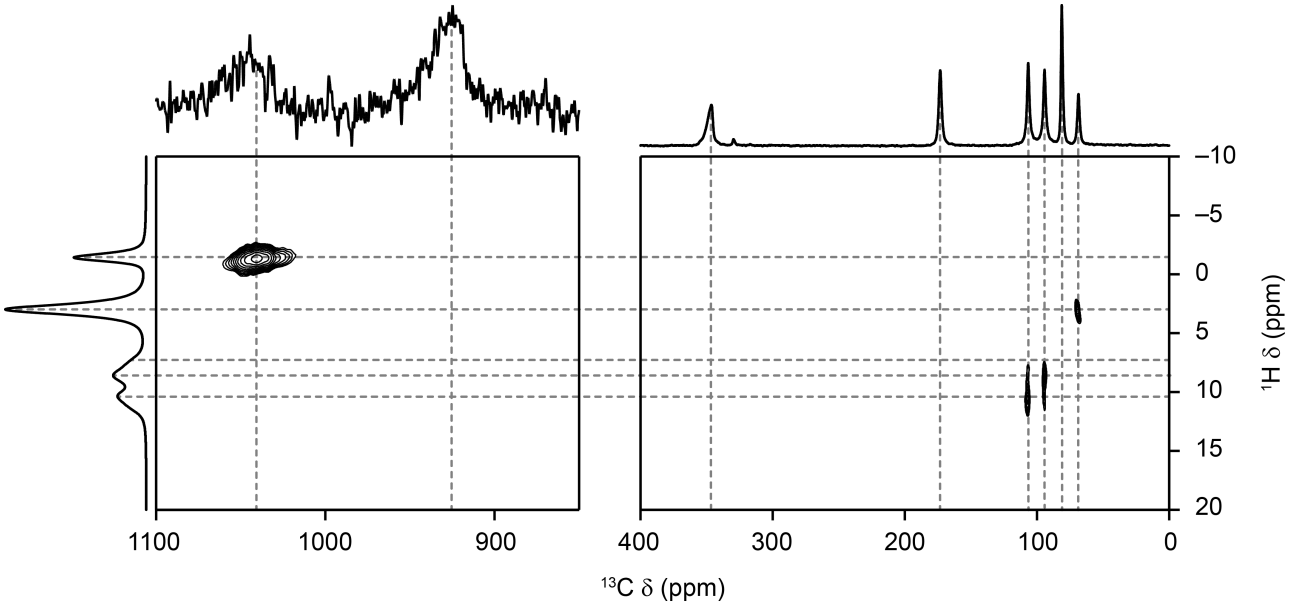

Fig. S4.10. ^{1}H-^{13}C (14.1 T, 298 K, 37.5 kHz MAS) CP HETCOR spectrum of **7**.

Fig. S4.11 shows the ^{1}H and ^{13}C MAS NMR spectra of **8**. Fig. S4.12 shows the ^{1}H-^{13}C CP HETCOR spectrum of **8**.

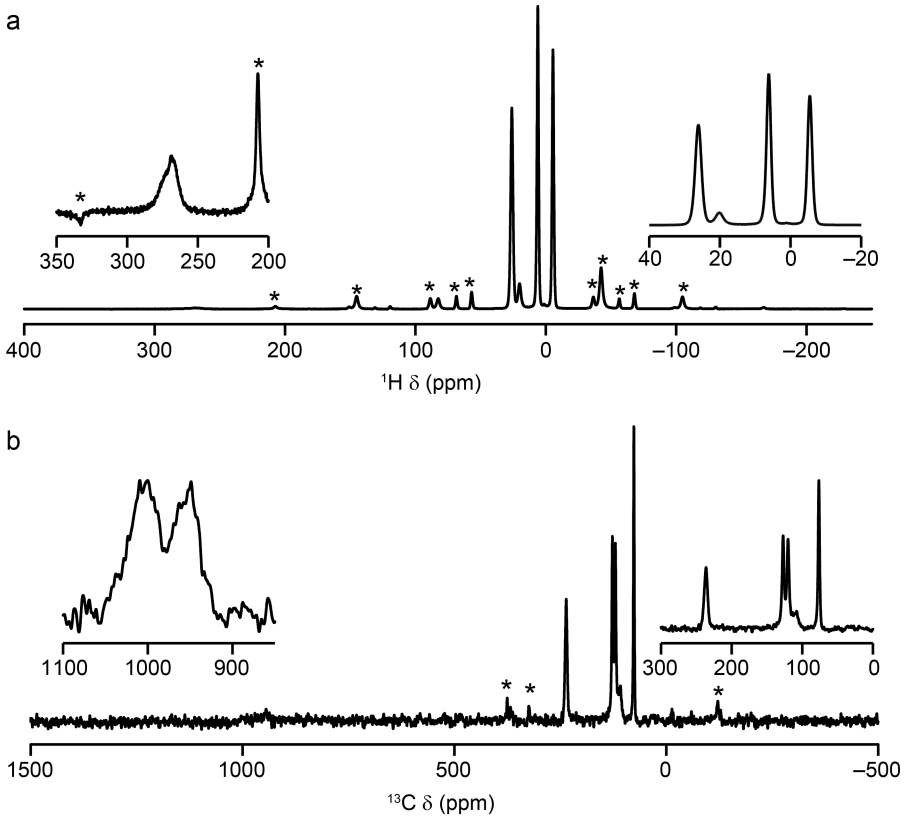

Fig. S4.11. (a) ^{1}H (14.1 T, 298 K, 37.5 kHz MAS) and (b) ^{13}C (14.1 T, 298 K, 37.5 kHz MAS) NMR spectra of **8**. Insets show expansions of the most shifted and more closely-spaced resonances. Spinning sidebands are marked by asterisks.

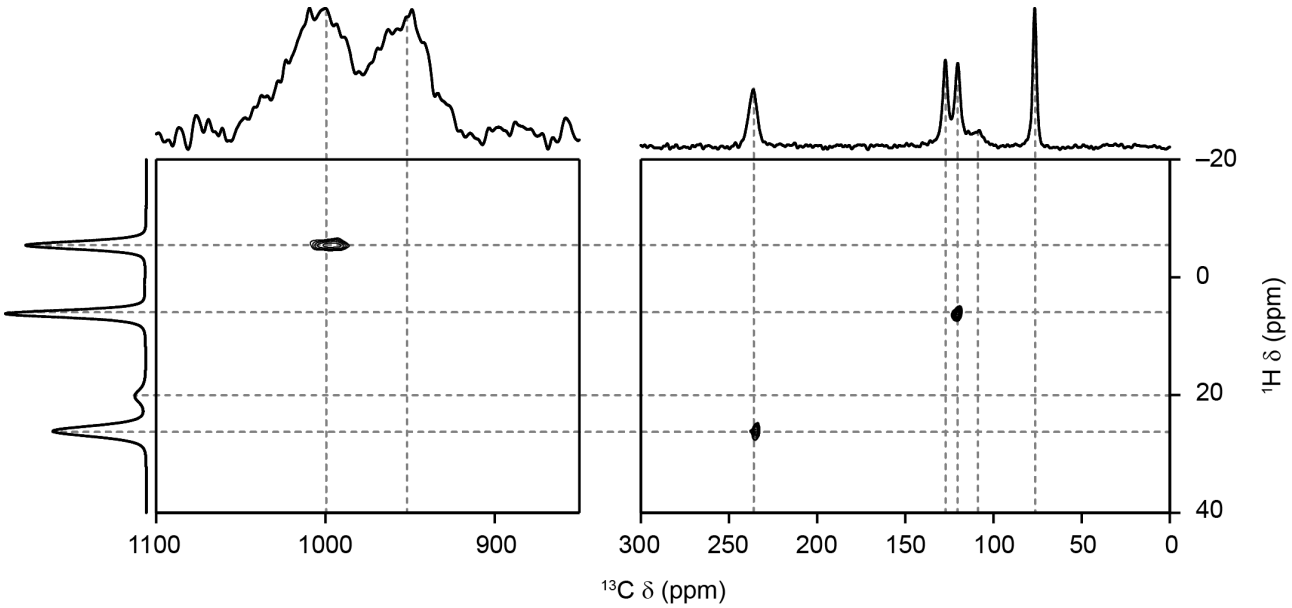

Fig. S4.12. ^{1}H-^{13}C (14.1 T, 298 K, 37.5 kHz MAS) CP HETCOR spectrum of **8**.

Fig. S4.13 shows the ^{1}H and ^{13}C MAS NMR spectra of **9**. Fig. S4.14 shows the ^{1}H-^{13}C CP HETCOR spectrum of **9**.

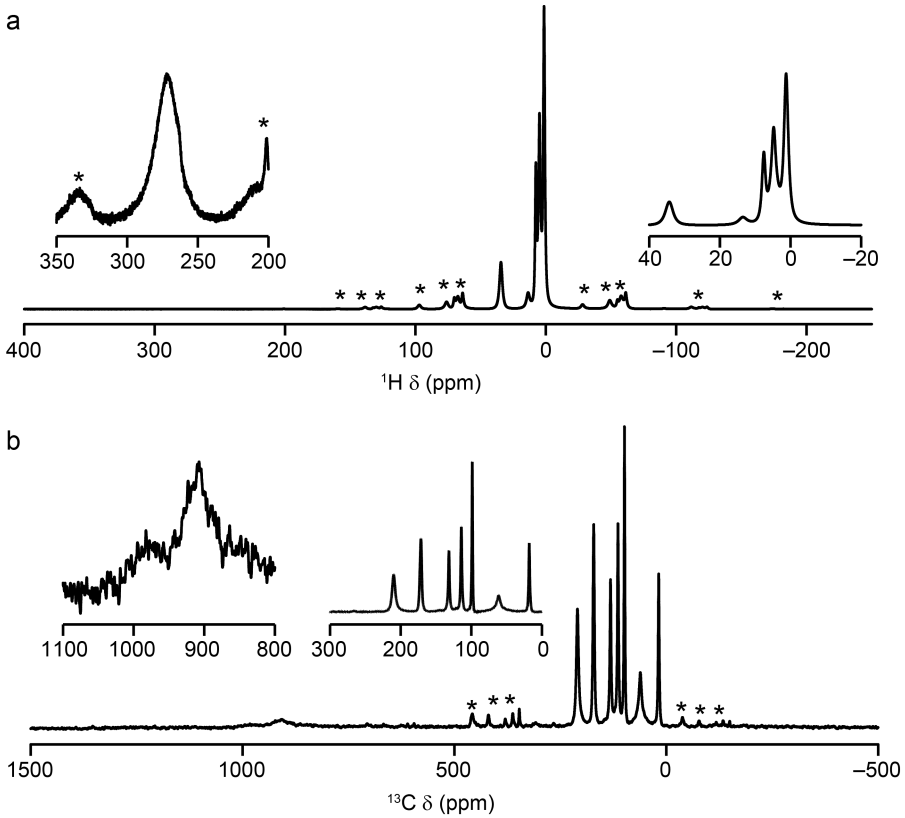

Fig. S4.13. (a) ^{1}H (14.1 T, 298 K, 37.5 kHz MAS) and (b) ^{13}C (14.1 T, 298 K, 37.5 kHz MAS) NMR spectra of **9**. Insets show expansions of the most shifted and more closely-spaced resonances. Spinning sidebands are marked by asterisks.

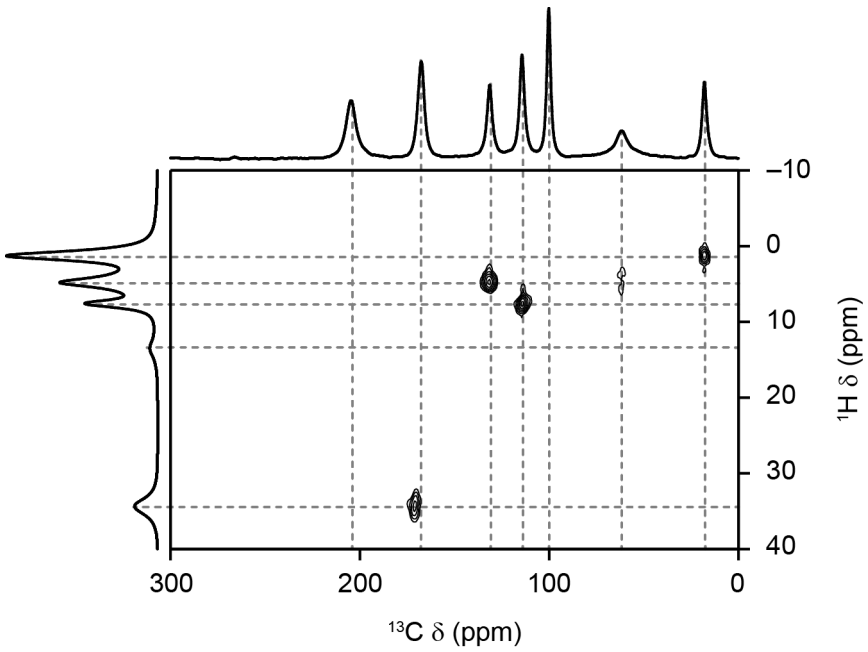

Fig. S4.14. ^{1}H-^{13}C (14.1 T, 298 K, 37.5 kHz MAS) CP HETCOR spectrum of **9**.

S5. Final Assignments of ^{1}H and ^{13}C NMR Spectra of 1-9.

The following tables report the experimental (exp.) and calculated (DFT) pNMR parameters for **1**-**5** and **7**-**9** (see Table 1 of the main text for the equivalent values for **6**). Resonances were assigned by achieving the best overall agreement between experimental and calculated values, taking into account connectivity information from the CP HETCOR spectra, as described in the main text. The standard error in the linear regression of a plot of δ_{iso} against $1/T$ is quoted in parentheses.

Table S5.1. pNMR parameters (as defined in the main text) for **1**.[S1]

Species	δ_{iso} at 298 K (ppm)		$d\delta_{iso}/d(1/T)$ / ppm K		δ_{iso}^{∞} (ppm)	
	exp.	DFT	exp.	DFT	exp.	DFT
H3	–5.4(1)	–6.81	$-3.03(2) \times 10^3$	-4.11×10^3	4.76(5)	6.98
H4	26.0(1)	26.0	$6.3\ (3) \times 10^3$	8.21×10^3	4.8(8)	7.47
H5[a]	5.5(1)	6.52	$1.6(3) \times 10^2$	–86.7	4.95(9)	6.81
H6[a]	5.5(1)	13.4	$1.6(3) \times 10^2$	1.85×10^2	4.95(9)	7.20
H7	272(2)	306.6	$8.87(8) \times 10^4$	8.89×10^4	–26(3)	8.30
Hbr	22.7(3)	22.7	$4.24(9) \times 10^3$	6.30×10^3	8.4(3)	10.59
C1	148(1)	132.2	$3.0(1) \times 10^3$	3.88×10^3	137.4(4)	119.2
C2	79.0(5)	79.4	$-1.403(3) \times 10^4$	-2.66×10^4	126.1(1)	168.4
C3	1006(5)	1167	$3.4(2) \times 10^5$	3.10×10^5	–115(51)	126.9
C4	244(1)	235.2	$3.89(4) \times 10^4$	2.82×10^4	114(1)	140.5
C5[b]	124(1)	144.7	$-8.6(6) \times 10^2$	7.11×10^3	126.9(2)	120.9
C6[b]	118(1)	108.7	$-1.33(5) \times 10^3$	-9.22×10^3	122.3(1)	139.6
C7	963(5)	931.5	$2.6(3) \times 10^5$	2.30×10^5	90(84)	159.1

a. H5 and H6 are not experimentally distinct, but have different calculated pNMR parameters.

b. C5 and C6 could not be assigned in our earlier work[S1] and the assignment may be reversed.

Table S5.2. pNMR parameters (as defined in the main text) for **2**.

Species	δ_{iso} at 298 K (ppm)		$d\delta_{iso}/d(1/T)$ / ppm K		δ_{iso}^{∞} (ppm)	
	exp.	DFT	exp.	DFT	exp.	DFT
H3	–1.8	–3.7	$-2.40(4) \times 10^3$	-3.19×10^3	6.3(1)	7.00
H4	28.6	35.2	$5.85(4) \times 10^3$	8.29×10^3	9.0(1)	7.41
H5	5.2	6.7	$1.4(3) \times 10^2$	–27.7	4.8(1)	6.81
H6	10.7	15.1	$1.26(1) \times 10^3$	2.24×10^3	6.48(5)	7.60
H8	–14.9	–29.0	$-5.33(5) \times 10^3$	-9.38×10^3	3.0(2)	2.50
Hbr	31.7	28.3	$6.3(1) \times 10^3$	5.03×10^3	10.5(3)	11.40
C1	110	120.1	$-5.31(5) \times 10^3$	-2.96×10^2	127.4(2)	121.1
C2	81	84.5	$-1.18(2) \times 10^4$	-2.46×10^4	120.4(8)	167.2
C3[a]	–	1146	–	3.04×10^5	–	127.2
C4	248	270.4	$3.25(7) \times 10^4$	3.91×10^4	138(2)	139.1
C5	133	136.6	$3.211(6) \times 10^3$	4.78×10^3	122.07(2)	120.6
C6	76	77.3	$-1.3(1) \times 10^4$	-1.74×10^4	118(4)	135.6
C7[a]	–	951.7	–	2.34×10^5	–	166.1
C8	284	459.0	$4.56(3) \times 10^4$	1.33×10^5	131(1)	13.6

a. not observed experimentally, perhaps owing to very rapid T_1 relaxation.

Table S5.3. pNMR parameters (as defined in the main text) for **3**. Where multiple resonances are observed for one chemical species, these are denoted ′. The complex has C_2 symmetry in the gas-phase calculation, so no such inequivalences are predicted by DFT.

Species	δ_{iso} at 298 K (ppm)		$d\delta_{iso}/d(1/T)$ / ppm K		δ_{iso}^{∞} (ppm)	
	exp.	DFT	exp.	DFT	exp.	DFT
H3	–5.3	–8.2	$-2.63(6) \times 10^3$	-4.59×10^3	3.5(2)	7.20
H3′	–5.8	–8.2	$-3.02(6) \times 10^3$	-4.59×10^3	4.4(2)	7.20
H4	35.9	43.0	$8.2(2) \times 10^3$	1.05×10^4	8.3(8)	7.95
H4′	33.6	43.0	$7.9(2) \times 10^3$	1.05×10^4	7.0(7)	7.95
H7	277	303.7	$7.9(1) \times 10^4$	8.77×10^4	12(3)	9.52
H7′	268	303.7	$7.5(1) \times 10^4$	8.77×10^4	13(4)	9.52
H8	7.5	9.5	266(7)	470	6.61(2)	7.88
H9	6.45	7.0	199(8)	–142	5.79(3)	7.48
H10	10.2	10.5	$8.1(2) \times 10^2$	830	7.49(7)	7.72
H11	6.5	8.0	269(8)	–48	5.60(3)	8.16
H11′	4.9	8.0	–37(11)	–48	5.02(4)	8.16
Hbr	12.3	33.5	$5.7(8) \times 10^2$	6.96×10^3	10.5(3)	10.17
C1	90	122.5	$-6.09(8) \times 10^3$	4.11×10^3	110.6(3)	108.7
C2	107	138.1	$-6.18(4) \times 10^3$	-9.42×10^3	127.8(1)	169.7
C2′	103	138.2	$-7.52(6) \times 10^3$	-9.42×10^3	127.8(2)	169.7
C3	1055	1209	$2.70(2) \times 10^5$	3.22×10^5	151(7)	129.3
C4	279	266.7	$4.29(2) \times 10^4$	3.71×10^4	135.1(7)	142.2
C5	169	156.0	$8.14(5) \times 10^3$	7.35×10^3	142.0(2)	131.4
C6	74	86.0	$-1.22(1) \times 10^4$	-1.58×10^4	114.9(4)	138.8
C7	1003	932.3	$2.53(2) \times 10^5$	2.32×10^5	151(7)	154.6
C8	124	127.4	$-1.12(9) \times 10^3$	-2.48×10^3	127.5(3)	135.7
C9	132	142.4	$1.0(3) \times 10^2$	4.39×10^3	132.0(1)	127.7
C9′	128.2	142.4	$-7.5(5) \times 10^2$	4.39×10^3	130.7(2)	127.7
C10	129	120.4	$2.5(3) \times 10^3$	-4.06×10^3	121(1)	134.1
C10′	128.1	120.4	$1.7(8) \times 10^3$	-4.06×10^3	122(3)	134.1
C11	121	142.4	$-1.5(1) \times 10^3$	5.57×10^3	126.2(3)	123.7

Table S5.4. pNMR parameters (as defined in the main text) for **4**.

Species	δ_{iso} at 298 K (ppm)		$d\delta_{iso}/d(1/T)$ / ppm K		δ_{iso}^{∞} (ppm)	
	exp.	DFT	exp.	DFT	exp.	DFT
H4	36.6	40.2	$9.25(8) \times 10^3$	9.96×10^3	5.6(3)	6.76
H5	8.1	5.0	$4.3(2) \times 10^2$	–513	6.67(7)	6.74
H6	5.4	12.3	$1.1(4) \times 10^2$	1.64×10^3	5.0(1)	6.81
H7	276	309	$7.9(3) \times 10^4$	8.96×10^4	12(10)	8.16
H8	4.3	4.0	141(6)	8.77×10^4	3.78(2)	3.61
Hbr	9.4	32.0	$-8.1(2) \times 10^2$	6.33×10^3	12.16(7)	10.79
C1	95	131.1	$-7.95(8) \times 10^3$	3.61×10^3	121.4(3)	119.0
C2	210	175.9	$2.42(1) \times 10^4$	5.13×10^3	128.4(3)	158.7
C3	922	1060	$2.1(1) \times 10^5$	2.69×10^5	211(31)	156.8
C4	167	163.7	$1.639(5) \times 10^4$	1.42×10^4	110.0(2)	116.0
C5	121	149.2	$1.31(6) \times 10^3$	8.74×10^3	116.1(2)	119.9
C6	132	99.8	$2.58(7) \times 10^3$	-8.84×10^3	123.0(2)	129.5
C7	944	920	$2.47(6) \times 10^5$	2.27×10^5	116(21)	158.1
C8	58	47.3	$-2.0(4) \times 10^2$	2.23×10^3	59.0(1)	54.8

Table S5.5. pNMR parameters (as defined in the main text) for **5**. Where multiple resonances are observed for one chemical species, these are denoted ′. The complex has C_2 symmetry in the gas-phase calculation, so no such inequivalences are predicted by DFT.

Species	δ_{iso} at 298 K (ppm)		$d\delta_{iso}/d(1/T)$ / ppm K		δ_{iso}^{∞} (ppm)	
	exp.	DFT	exp.	DFT	exp.	DFT
H3	–6.0	–6.9	$-3.29(4) \times 10^3$	-4.14×10^3	5.0(1)	6.95
H4	30.0	35.4	$6.81(7) \times 10^3$	8.23×10^3	7.2(2)	7.58
H6	10.7	13.4	$7.9(2) \times 10^2$	1.88×10^3	12.6(1)	7.13
H7	271	306	$6.8(2) \times 10^4$	8.87×10^4	43(7)	8.12
H9	2.0	1.2	207(9)	–19.5	1.29(3)	1.24
H9′	1.9	1.2	$1.8(3) \times 10^2$	–19.5	1.22(9)	1.24
Hbr	7.5	31.1	$3.0(1) \times 10^2$	6.12×10^3	6.51(3)	10.56
C1	107	131.0	$-8.0(2) \times 10^3$	3.93×10^3	134.0(5)	117.8
C2	94	77.1	$-8.43(9) \times 10^3$	-2.67×10^4	122.5(3)	166.8
C2′	91	77.1	$-8.9(1) \times 10^3$	-2.67×10^4	121.0(3)	166.8
C3	1326	1070	$7(2) \times 10^5$	3.11×10^5	–1020(790)	126.1
C4	233	231.7	$3.03(4) \times 10^4$	2.75×10^4	131(1)	139.4
C5	149	168.6	$7.2(3) \times 10^2$	7.53×10^3	146.92(9)	143.3
C6	117	101.0	$-9.2(5) \times 10^2$	-1.00×10^4	120.2(2)	134.7
C6′	115	101.0	$-3.4(1) \times 10^3$	-1.00×10^4	126.6(3)	134.7
C7	1013	937	$2.4(3) \times 10^5$	2.32×10^5	186(93)	158.9
C8	37	35.4	$1.13(1) \times 10^3$	–65.8	33.08(4)	35.6
C9	35	34.1	$-3.5(3) \times 10^2$	450	36.01(9)	32.6

Table S5.6. pNMR parameters (as defined in the main text) for **7**.

Species	δ_{iso} at 298 K (ppm)		$d\delta_{iso}/d(1/T)$ / ppm K		δ_{iso}^{∞} (ppm)	
	exp.	DFT	exp.	DFT	exp.	DFT
H3	–1.4	–2.7	$-1.94(1) \times 10^3$	-2.67×10^3	5.12(4)	6.22
H5	8.7	5.7	$8.4(2) \times 10^2$	–235	5.84(6)	6.46
H6	10.5	11.1	$1.17(7) \times 10^3$	1.22×10^3	6.5(2)	7.03
H7	274	302	$8.1(1) \times 10^4$	8.76×10^4	2(3)	7.99
H8	3.0	2.2	$-1.5(1) \times 10^2$	–403	3.54(5)	3.58
Hbr	7.7	32.5	$6.6(2) \times 10^2$	6.65×10^3	5.5(5)	10.19
C1	173	112.5	$1.065(8) \times 10^4$	102	137.6(3)	112.2
C2	81	143.8	$-9.90(6) \times 10^3$	-8.06×10^3	114.6(2)	170.8
C3	1047	1209	$2.84(8) \times 10^5$	3.29×10^5	95(25)	104.7
C4	347	329.6	$5.74(5) \times 10^4$	4.74×10^4	155(2)	170.5
C5	94	127.8	$-4.80(8) \times 10^3$	4.71×10^3	110.5(3)	112.1
C6	107	102.2	$-7.17(6) \times 10^3$	-1.14×10^4	130.8(2)	140.6
C7	928	928	$2.41(5) \times 10^5$	2.29×10^5	119(16)	157.8
C8	69	61.4	$4.40(6) \times 10^3$	1.96×10^3	54.0(2)	54.8

Table S5.7. pNMR parameters (as defined in the main text) for **8**.

Species	δ_{iso} at 298 K (ppm)		$d\delta_{iso}/d(1/T)$ / ppm K		δ_{iso}^{∞} (ppm)	
	exp.	DFT	exp.	DFT	exp.	DFT
H3	–5.4	–6.8	$-2.71(5) \times 10^3$	-4.09×10^3	3.7(2)	6.88
H4	26.1	34.0	$5.24(5) \times 10^3$	7.92×10^3	8.5(1)	7.46
H6	6.2	14.4	$1.2(2) \times 10^2$	2.15×10^3	5.82(8)	7.23
H7	269	308.4	$7.7(5) \times 10^4$	8.95×10^4	13(17)	8.06
Hbr	20.2	32.4	$2.24(3) \times 10^3$	6.54×10^3	12.6(1)	10.49
C1	127	129.1	$-4.2(1) \times 10^3$	2.62×10^3	141.5(4)	120.3
C2	77	83.4	$-1.23(2) \times 10^4$	-2.49×10^4	118.0(6)	167.1
C3	1005	1178	$2.55(5) \times 10^5$	3.13×10^5	148(15)	127.3
C4	236	234.6	$2.96(5) \times 10^4$	2.70×10^4	137(2)	143.8
C5	109	153.4	$-3.2(7) \times 10^3$	7.70×10^3	120(2)	127.5
C6	120	100.9	$-2.53(8) \times 10^3$	-1.23×10^4	128.8(2)	142.2
C7	951	895	$2.41(2) \times 10^5$	2.20×10^5	143(7)	158.2

Table S5.8. pNMR parameters (as defined in the main text) for **9**.

Species	δ_{iso} at 298 K (ppm)		$d\delta_{iso}/d(1/T)$ / ppm K		δ_{iso}^{∞} (ppm)	
	exp.	DFT	exp.	DFT	exp.	DFT
H4	34.4	40.0	$8.1(1) \times 10^3$	9.92×10^3	7.2(4)	6.74
H5	4.8	4.9	$1.5(2) \times 10^2$	–534	4.28(7)	6.72
H6	7.6	12.3	$2.9(1) \times 10^2$	1.65×10^3	6.62(5)	6.79
H7	272	309	$7.9(3) \times 10^4$	8.95×10^4	6(8)	8.17
H8	4.8	4.3	$1.5(2) \times 10^2$	188	4.28(7)	3.66
H9	1.3	1.0	–83(26)	–117	1.55(9)	1.41
Hbr	13.6	31.8	189(7)	6.25×10^3	12.96(2)	10.86
C1	99	131.3	$-6.39(8) \times 10^3$	3.69×10^3	120.4(3)	118.9
C2	210	175.2	$2.49(3) \times 10^4$	5.00×10^3	126.5(8)	158.4
C3	907	1055	$2.1(1) \times 10^5$	2.68×10^5	195(31)	156.3
C4	172	163.9	$1.90(2) \times 10^4$	1.42×10^4	107.9(5)	116.4
C5	132	149.7	$2.1(1) \times 10^3$	8.88×10^3	124.8(4)	119.9
C6	114	98.9	$-3.0(8) \times 10^2$	-9.04×10^3	115.4(3)	129.2
C7	980	919	$2.4(1) \times 10^5$	2.27×10^5	187(37)	158.1
C8	62	56.8	$-1(3) \times 10^3$	-2.13×10^3	64.8(9)	63.9
C9	18	15.1	$5(1) \times 10^2$	–289	16.3(4)	16.1

S6. Vibrational Effects on the pNMR Parameters of 1

To investigate possible effects of vibrational averaging on the chemical shifts of **1** the effective zero-point averaged structure (r_g^0 structure) was computed from the cubic force field using the method of Barone *et al*.[S29] The cubic force field was evaluated through numerical differentiation of harmonic second derivatives within Gaussian 09[S13] at the same PBE0-D3/Wachters/6-31G*(*) level used for structure optimisation (using tight optimisation criteria through the `opt=tight` option), employing the default values for step size in the numerical differentiation (0.025Å) and the integration grid. pNMR shifts were computed for this zero-point averaged structure at the PBE0-1/3/II level (and referenced to TMS, which was vibrationally averaged the same way). This method has been used previously to assess the effects of vibrational averaging on structural and NMR parameters of diamagnetic transition metal complexes.[S30] The results are summarised in Table S6.1.

As expected from the increase in r_g^0 over r_e bond lengths and the usual tendency towards decreased shielding with increased bond distances, most resonances have a slightly larger shift upon vibrational averaging. Notable exceptions are the strongly deshielded C3 and C7 resonances, which become more shielded (by up to 3 ppm), and Hbr, which is 2.5 ppm more shielded. The latter change is quite substantial for a ^{1}H shift and could point to a strongly anharmonic stretching potential of the corresponding bond, which would not be unusual for protons involved in strong, possibly low-barrier hydrogen bonds. Inspection of the vibrationally averaged OH distances involved in the intramolecular H-bond, however, shows only minor changes from the optimised equilibrium values (around 0.003 Å, see Table S6.2).

When the stretching potential for simultaneous compression and elongation of the two O-Hbr bonds was computed explicitly (through optimising all other parameters at the PBE0-D3/Wachters/6-31G*(*) level in C_{2h} symmetry), the potential shown in Fig. S6.1 was obtained. It shows the characteristic of a deep single well, where distinct deviations from a

"normal" Morse-type potential (dotted curve in Fig. S6.1) are only apparent at large OH distances and rather high energies. The notable effect of vibrational averaging on the shift of Hbr (Table S6.1) thus appears to be due to a strong structural sensitivity of this property (rather than large structural changes upon vibrational averaging). This interpretation is consistent with the location of this proton in an area of strongly variable spin density (*cf.* Fig. 2b of the main text), where relatively small displacements (*cf.* Table S6.2) can result in relatively large variations of the magnetic shielding and, arguably, of its temperature dependence.

Table S6.1. Computed pNMR chemical shifts[a] (in ppm relative to TMS)[b] for **1** in its equilibrium (r_e) and zero-point averaged structures (r_g^0).

Species	δ_{iso} (ppm)	
	r_e	r_g^0
H3	–6.8	–6.6
H4	35.0	35.6
H5	6.5	6.9
H6	13.4	13.8
H7	306.6	308.2
Hbr	31.7	29.2
C1	132.4	134.5
C2	79.2	79.9
C3	1166.6	1164.7
C4	235.3	237.3
C5	144.8	147.4
C6	108.8	110.7
C7	931.4	930.8

a. PBE0-⅓/IGLO-II level, doublet state.

b. Averaged σ_{iso} for TMS: ^{1}H 31.8 ppm, ^{13}C 189.0 ppm at equilibrium, ^{1}H 32.14 ppm, ^{13}C 190.88 ppm at 0 K.

Table S6.2. Distances (in Å) between bridging hydrogen and its neighboring oxygens.[a]

Bond	r_e	r_g^0
O-Hbr	0.987	0.990
O···Hbr	1.724	1.727

a. PBE0-D3/Wachters/6-31G*(*) level.

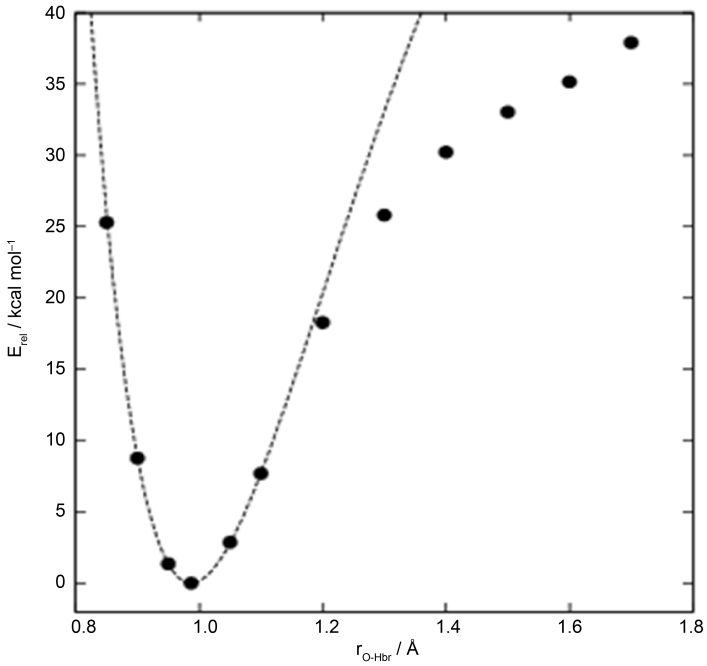

Fig. S6.1. PBE0-D3/Wachters/6-31G*(*) energy as a function of the two O-Hbr distances (kept equal, all other parameters optimised); dotted line: fit of a Morse potential to the five points below 10 kcal mol^{-1}.

The zero-point averaged structure is still planar. To probe to what extent out-of-plane twists could affect the pNMR shifts a relaxed energy scan was carried out along a suitable reaction coordinate and computed the shieldings for these twisted structures. The chosen coordinate comprised the Oa-C1-C1′-Oa′ and Nb-C1-C1′-Nb′ dihedral angles, which were fixed to the same value θ (see Fig. S6.2(a) for the numbering scheme used here). In addition, the C1-Cu-C1′ angle was kept fixed at 180° to ensure a smooth transition between the planar and a pseudo-tetrahedral coordination geometry about Cu; all other parameters were optimised at the PBE0-D3/Wachters/6-31G*(*) level. As

expected for a d^9 complex from the first transition row, the pseudo-tetrahedral structure with θ = 90° is very high in energy (32.3 kcal mol^{-1} above the minimum at θ = 180°), but quite noticeable distortions up to θ = 155° cost less than 4 kcal mol^{-1} (see Fig. S6.2(b)).

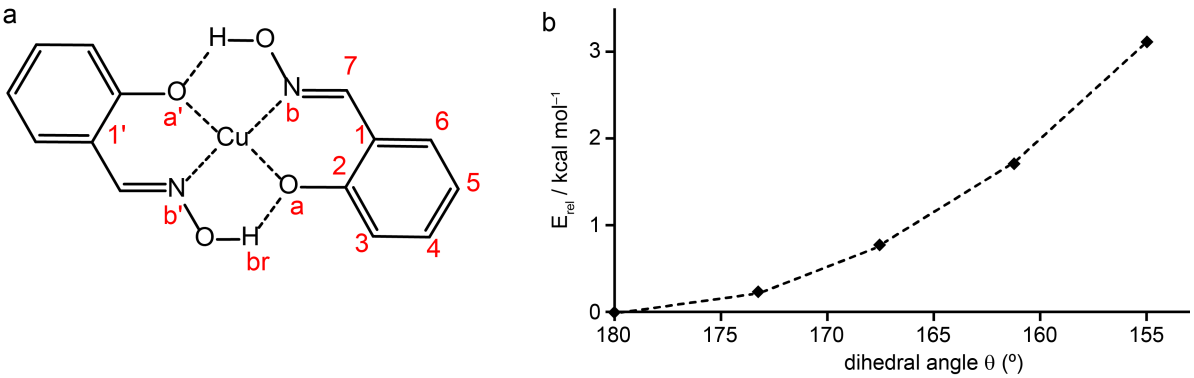

Fig. S6.2. (a) Numbering scheme for **1**, including for the N and O atoms. (b) PBE0-D3/Wachters/6-31G*(*) energy as a function of the two Oa-C1-C1′-Oa′ and Nb-C1-C1′-Nb′ dihedral angles.

The pNMR chemical shifts computed for these twisted structures are given in Table S6.3 and the resulting schematic NMR spectra as a function of the twist are plotted in Fig. S6.3. There are noticeable shifts of some signals with increasing twist, notably for Hbr, C7 and C2. In many cases, the trends are opposite to those of the full zero-point vibrational averaging given in Table S6.1 (*e.g.*, Hbr is predicted to be shielded by full vibrational averaging,[S31] but deshielded by out-of-plane twists; but *vice* versa for H7). Full appraisal would require a dynamical study (preferably including nuclear dynamics),[S32] which is beyond the scope of the present paper.

Table S6.3. Computed pNMR chemical shifts[a] (in ppm relative to TMS) for complex **1** as a function of dihedral twist angle θ.

Species	θ (°)				
	180.00	173.75	167.50	161.25	155.00
H3	–6.8	–7.1	–7.2	–7.7	–8.4
H4	35.0	35.0	34.8	34.6	34.3
H5	6.5	6.4	6.0	5.4	4.5
H6	13.4	13.4	13.6	13.9	14.5
H7	306.6	305.1	303.0	299.0	293.7
Hbr	31.7	34.2	36.9	50.2	61.5
C1	132.2	132.1	132.8	133.0	135.1
C2	79.4	73.1	49.9	9.2	–39.9
C3	1166.5	1164.1	1163.4	1155.4	1147.1
C4	235.2	234.0	232.0	227.1	220.7
C5	144.7	145.3	146.6	149.7	154.2
C6	108.7	107.9	105.6	100.9	94.4
C7	931.5	919.3	896.8	851.2	797.5

a. PBE0-1/3/IGLO-II level.

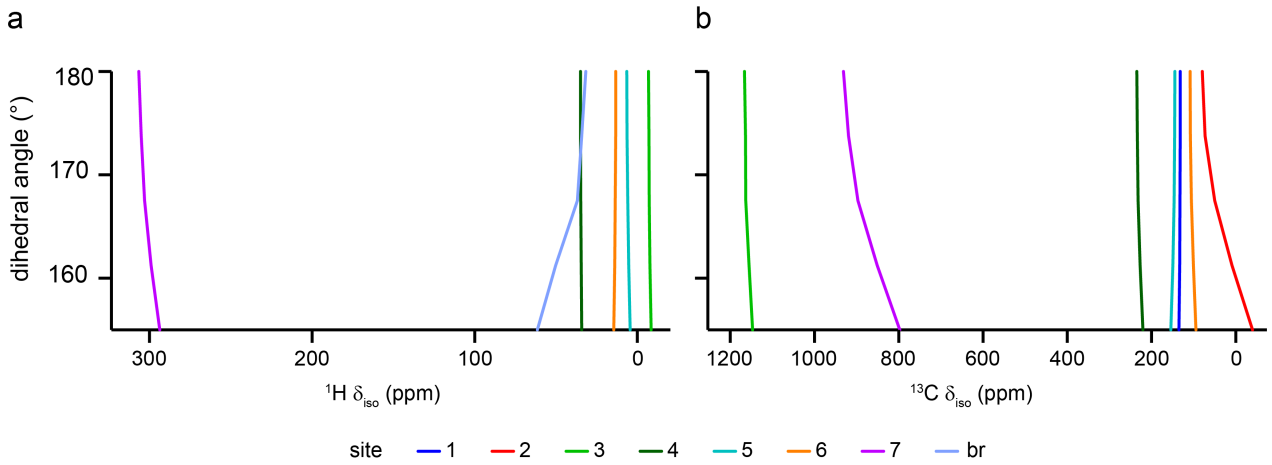

Fig. S6.3. Plots of computed (a) ^{1}H and (b) ^{13}C isotropic shifts (at 298.15 K) as a function of the dihedral twist angle θ. For numerical values, see Table S6.3.

S7. References

S1. M. Bühl, S. E. Ashbrook, D. M. Dawson, R. A. Doyle, P. Hrobárik, M. Kaupp and I. A. Smellie, *Chem. Eur. J.*, 2016, **22**, 15328.

S2. N. Otto and T. Opatz, *Beilstein J. Org. Chem*., 2012 , **8**, 1105.

S3. C. E. Coulthard, J. Marshall and F. L. Pyman, *J. Chem. Soc.*, 1930, 280.

S4. H. A. Torrey and C. M. Brewster, *J. Am. Chem. Soc*., 1913, **35**, 426.

S5 L. Rupp, *Arch. Pharm.*, 1915, **253,** 34

S6. I. A. Smellie, R. S. Forgan, C. Brodie, J. S. Gavine, L. Harris, D. Houston, A. D. Hoyland, R. P. McCaughan, A. J. Miller, L. Wilson and F. M. Woodhall, *J. Chem. Educ*., 2016, **93**, 362.

S7. D. Stepniak-Biniakiewicz, *Pol. J. Chem*., 1980, **54**, 7.

S8. Patent WO2004/67518 A1,Bayer Cropscience Aktiengesellschaft, 2004.

S9. N. Gigant, E. Claveau, P. Bouyssou and I. Gillaizeau, *Org. Lett*., 2012, **14**, 844.

S10. M. Dolai, T. Mistri, S. Biswas, G. Rogez and M. Ali, *ChemPlusChem*, 2014, **79**, 1649.

S11. K. N. Lazarou, A. K. Boudalis, V. Psycharis and C. P. Raptopoulou, *Inorg. Chim. Acta*, 2011, **370**, 50.

S12. F. M. Mack, *MChem Thesis*, University of St Andrews, 2017.

S13. Gaussian 09, Revision B.01, M. J. Frisch, G. W. Trucks, H. B. Schlegel, G. E. Scuseria, M. A. Robb, J. R. Cheeseman, G. Scalmani, V. Barone, B. Mennucci, G. A. Petersson, H. Nakatsuji, M. Caricato, X. Li, H. P. Hratchian, A. F. Izmaylov, J. Bloino, G. Zheng, J. L. Sonnenberg, M. Hada, M. Ehara, K. Toyota, R. Fukuda, J. Hasegawa, M. Ishida, T. Nakajima, Y. Honda, O. Kitao, H. Nakai, T. Vreven, J. A. Montgomery, Jr., J. E. Peralta, F. Ogliaro, M. Bearpark, J. J. Heyd, E. Brothers, K. N. Kudin, V. N. Staroverov, T. Keith, R. Kobayashi, J. Normand, K. Raghavachari, A. Rendell, J. C. Burant, S. S. Iyengar, J. Tomasi, M. Cossi, N. Rega, J. M. Millam, M. Klene, J. E. Knox, J. B. Cross, V. Bakken, C. Adamo, J. Jaramillo, R. Gomperts, R. E. Stratmann, O. Yazyev, A. J. Austin, R. Cammi, C. Pomelli, J. W. Ochterski, R. L. Martin, K. Morokuma, V. G. Zakrzewski, G. A. Voth, P. Salvador, J. J. Dannenberg, S. Dapprich, A. D. Daniels, O. Farkas, J. B. Foresman, J. V. Ortiz, J. Cioslowski and D. J. Fox, Gaussian, Inc., Wallingford CT, 2013.

S14. J. P. Perdew, In Electronic Structure of Solids, Ziesche, P.; Eischrig, H. Eds.: Akademie Verlag: Berlin (1991).

S15. J. P. Perdew and Y. Wang, *Phys. Rev. B* 1992, **45**, 13244.

S16. J. P. Perdew, M. Ernzerhof and K. Burke, *J. Phys. Chem*. 1996, **105**, 9982.

S17. C. Adamo and V. Barone, *J. Chem. Phys*. 1999, **110**, 6158.

S18 S. Grimme, J. Antony, S. Ehrlich and H. Krieg, *J. Chem. Phys.* 2010, **132**, 154104.

S19. A. D. Becke and E. R. Johnson, *J. Chem. Phys.* 2005, **122**, 154104.

S20. E. R. Johnson and A. D. Becke, *J. Chem. Phys.* 2006, **124**, 174104.

S21. A. J. H. Wachters, *J. Chem. Phys.* 1970, 52, 1033.

S22. P. J. Hay, *J. Chem. Phys.* 1977, 66, 4377.

S23. C. A. Guido, E. Bremond, C. Adamo and P. Cortona, *J. Chem. Phys.* 2001, **138**, 201104.

S24. M. Munzarová and M. Kaupp, J. Phys. Chem. A 1999, 103, 9966.

S25. W. Kutzelnigg, U. Fleischer and M. Schindler, In: *NMR Basic Principles and Progress Vol. 23*, Springer-Verlag: Berlin, 1990, p. 165.

S26. Orca, Version 3.0.3: (a) F. Neese, *WIREs Comp. Mol. Sci* 2012, **2**, 73; (b) https://orcaforum.cec.mpg.de (accessed 20 May 2016).

S27. P. Hrobarik, R. Reviakine, A. V. Arbuznikov, O. L. Malkina, V. G. Malkin, F. Koehler and M. Kaupp. *J. Chem. Phys*. 2007, **126**, 024107.

S28. J. Skibsted and H. J. Jakobsen, *J. Phys. Chem. A*, 1999, **103**, 7958-7971.

S29. (a) V. Barone *J. Chem. Phys.* 2004, **120**, 3059. (b) V. Barone, *J. Chem. Phys.* 2005, **122**, 014108. See also: (c) K. Ruud, P.-O. Åstrand and P. R. Taylor, *J. Chem. Phys.* 2000, **112**, 2668. (d) K. Ruud, P.-O. Åstrand and P. R. Taylor, *J. Am. Chem. Soc.* 2000, **123**, 4826. (e) T. Ruden, O. B. Lutnæss and T. Helgaker, *J. Chem. Phys.* 2003, **118**, 9572.

S30. See *e.g.*, (a) M. Bühl, C. Reimann, D. A. Pantazis, T. Bredow and F. Neese, *J. Chem. Theory Comput*. 2008, **4**, 1449. (b) S. Grigoleit and M. Bühl, *Chem. Eur. J*., 2004, **10**, 5541.

S31. Note that full vibrational averaging would require expansion of the nuclear shielding surface about the effective (r_g^0) structure and perturbative inclusion of the resulting corrections to the effective shielding (σ_{eff}) at the r_g^0 structure (through the second derivative of the magnetic shielding surface, *cf.* references S29(d,e)); because this procedure is rather costly and usually produces only minor corrections to σ_{eff}

(especially for transition metal complexes, see: M. Bühl, P. Imhof and M. Repisky, *ChemPhysChem*. 2004, **5**, 414) it was not implemented here.

S32. For a path integral molecular dynamics study of ^{13}C δ_{iso} in diamagnetic molecular organic solids see: M. Dracinsky and P. Hodgkinson, *Chem. Eur. J.* 2014, **20**, 2201.